Available online at www.sciencedirect.com
ScienceDirect
Journal of Sound and Vibration 323 (2009) 574–593
JOURNAL OF SOUND AND VIBRATION
www.elsevier.com/locate/jsvi

Model based feed-forward control of electromagnetic type active control engine-mount system

Bo-Ha Lee, Chong-Won Lee*

Center for Noise and Vibration Control, Department of Mechanical Engineering, Korea Advanced Institute of Science and Technology, Science Town, Daejeon 305-701, South Korea

Received 28 May 2007; received in revised form 6 January 2009; accepted 19 January 2009
Handling Editor: J. Lam
Available online 25 February 2009

Abstract

This paper introduces a low-cost prototype active control engine mount (ACM) designed for commercial passenger vehicles, requiring a good engine vibration isolation performance. To construct such an ACM system, all feedback sensors normally required for full ACM systems are replaced by the model based feed forward algorithm, consisting of a vibration estimation algorithm, a current shaping controller and an enhanced ACM model. The ACM model describes the active as well as passive characteristics of ACM. The current shaping control compensates for degradation of control performance due to elimination of feedback control sensors. The engine vibration estimator, which uses such existing sensors as CAM and crank angle sensor (CAS), replaces a sensor to monitor the transmitted vibrations from the engine to the chassis. The validity of the ACM model is experimentally verified so that it accurately predicts the dynamic behaviors of the ACM over the frequency range of interest. The proposed current shaping control improves the actuator control performance, and the vibration estimation algorithm provides the anti-vibration signals for vibration isolation. Finally, it is experimentally proved that the vibration isolation performance of the developed ACM for the engine-induced vibration of interest can be improved by more than 13 dB.

1. Introduction

Engine mounts require two contradictory functions: efficient vibration isolation and firm engine support. The primary way to cut-off the paths of noise and vibration from engine is to use soft mounts with light damping. However, engine mounts must constrain or control engine excursions caused by rough roads, firing in cylinders, wheel torque reactions and so on. To limit the excessive engine motions, engine mounts should be stiff and heavily damped. These two conflicting requirements for the engine-mount design have promoted automotive industries to search for new engine-mounting methods [1–3].

One of the effective engine-mounting methods to meet those conflicting requirements is the use of an active control engine mount (ACM). Vibrations produced by an active system are controlled to cancel the primary

*Corresponding author. Tel.: +82 42 869 3016; fax: +82 42 869 8220.
E-mail addresses: cwlee@kaist.ac.kr, cwlee3016@gmail.com (C.-W. Lee).

0022-460X/$ - see front matter © 2009 Elsevier Ltd. All rights reserved.
doi:10.1016/j.jsv.2009.01.033

Nomenclature

A_c	decoupler area
A_e	equivalent piston area of rubber
A_p	pole face area
A_t	cross-sectional area of inertia track
$[C]$	damping matrix of engine-mounting system
C_b	volumetric compliance
f_c	control force of electromagnetic actuator
F	magnitude of control force
F_T	transmitted force through ACM
F_x	transmitted force to the engine
F_y	transmitted force to the chassis
g_0	nominal air gap
I	current of coil
$[K]$	stiffness matrix of engine-mounting system
K_c	stiffness of actuator
K_r	main stiffness of rubber
K_t	stiffness of diaphragm
K_{xx}	driving point dynamic stiffness at the engine side
K_{xy}, K_{yx}	transfer dynamic stiffness of ACM
K_{yy}	driving point dynamic stiffness at the chassis side
m	mass of engine-transmission block
m_c	mass of actuator runner
m_y	fluid mass of inertia track
$[M]$	inertia matrix of engine-mounting system
N	number of coil turns
P	pressure in the upper fluid chamber
R_c	damping of actuator
R_t	damping of inertia track
T_{xc}	force transmissibility at the engine side
T_{yc}	force transmissibility at the chassis side
x, X	vibration displacement of ACM at the engine side
x_c	displacement of actuator runner
x_t	displacement of fluid in inertia track
y, Y	vibration displacement of ACM at the chassis side
μ	absolute permeability
ϕ	phase of control force
Ω	frequency of control force

vibrations caused by the engine. For active vibration control, actuators create counteracting dynamic forces, in order to suppress the transmitted disturbance forces from the engine to the chassis. A typical ACM consists of a passive hydraulic engine mount (HEM), an active actuator and its electric controller. The electric controller provides control command signals to the active actuator, which produces the counteracting dynamic force, to minimize the transmitted force [4].

In recent years, various types of ACMs have been developed by many researchers. Ozaki [5] proposed an ACM that used a pneumatic actuator as an active system. The ACMs activated by piezo-electric actuators were developed by Haldenwanger and Klose [6], and, Ushijima and Jumakawa [7]. The electromagnetic type ACMs were evolved to utilize their high specific force per unit volume [8–12]. Recently, Japanese automotive companies such as Toyota [5], Nissan [11] and Honda [12] introduced ACMs to the automotive market. They provided the good vehicle tested mount results and highlighted improvements in isolation of force induced by engine roll motion over the low frequency region of interest.

In development of ACM, there are two important considerations: performance and cost. Engine mount should be cost-effective to be loaded on commercial passenger vehicles. Full loaded ACMs, normally requiring expensive sensors for feedback control, are not widely used for their high cost, even though they have excellent vibration isolation performances and thus significantly improve the NVH (noise, vibration and harshness) characteristics of vehicles.

This research mainly focuses on development of an ACM designed for low-cost and, yet satisfactory vibration isolation performance. A full loaded ACM system normally requires two sensors: one for measurement of engine vibration or transmitted force through ACM, and the other for position feedback of actuator itself. Without such sensors, the performance of ACM will degrade, compared with the full loaded ACM. In this paper, a model based feed forward algorithm, which consists of a vibration estimation algorithm, a current shaping controller and an improved ACM model, is adopted, in order to compensate for the performance degradation due to absence of the feedback sensors. The engine vibration estimator indirectly monitors the engine vibrations using the signals taken from the existing sensors such as CAM and CAS [12–14]. The current shaping controller compensates for the undesired harmonic distortion in the actuator

output due to lack of its position feedback. The improved ACM model is developed to accurately describe the active as well as passive characteristics of ACM.

A prototype ACM was developed and tested for the model verification and control performance evaluation in the laboratory. The model verification tests showed that the analytical model predicted the dynamic behaviors of the ACM over the frequency range of interest with fair accuracy. The control performance tests were carried out to evaluate the performances of the model based feed-forward controller with the prototype ACM. It was found that the proposed current shaping control significantly improved the actuator performance, the vibration estimation algorithm effectively provided anti-vibration signals for vibration isolation, and the prototype ACM successfully isolated the engine-induced vibrations.

2. Function and structure of ACM

2.1. Principal function of ACM

When an engine operates, the engine block is shaken by dynamic combustion torques generated from firing cylinders, and the resulting vibration transfers from the engine block to the chassis, passing through the mounts supporting the engine. The main function of ACM is to isolate the potential dynamic force transmitted from the engine to the chassis by properly activating an active device installed in the ACM system.

2.2. Structure of ACM

To isolate the engine-induced vibration, many researchers have developed various kinds of ACMs [6–11], but their basic structures are similar to each other, as illustrated in Fig. 1. ACM generates an anti-vibration force, canceling out the transmitted force from the engine to the chassis. In the conventional full loaded ACM system, the anti-vibration signal is obtained from direct measurement of engine vibration by using a sensor, and the actuator system requires an additional sensor for position feedback itself. These sensors, which are used for vibration monitoring and actuator control, make the full loaded ACM system expensive.

Recently, Japanese automotive companies (Toyota, Honda) have developed low-cost ACM systems without feedback sensors and applied them to commercial vehicles [5,12]. The main concerns in design of such cost-effective ACM systems were the engine vibration measurement for anti-vibration commands and the control command generation for producing the anti-vibration forces by the ACM actuator. These were achieved by different methods from the full loaded ACM system. First, instead of direct force measurement, the deviations

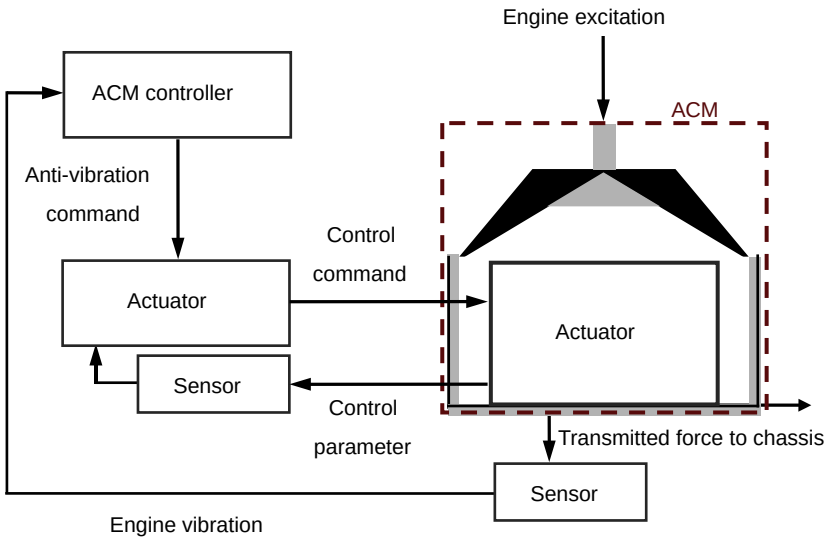

Fig. 1. Structure of the conventional full active control engine mount.

in the crack shaft rotation caused by engine combustion were detected from the CAS signals, and then a magnitude of engine vibration was estimated using a pre-built gain map between the measured forces to the chassis via ACM and the estimated vibration signals for varying engine speeds and operating conditions. And the CAM pulse signal was applied as the phase reference for control. Thus, the ACM system estimated the magnitude and phase of the engine vibrations, and, determined the anti-vibration commands. Second, the degeneration of performance of ACM actuator, caused by elimination of feedback control sensors, was compensated by adding a filter orifice above the actuator. Undesired harmonics due to the free vibration of actuating system was reduced to some extent by the filter orifice, but it increased the dynamic stiffness of the ACM system in the high frequency region, and then amplified the vibration transfer via the ACM. The low-cost ACMs provided good vibration isolation performance in vehicle tests, but there still remain problems in engine vibration estimation technique, controller of the ACM system and proper mathematical model for design and control.

In this paper, three major contributions are made. First, a refined ACM model, which accounts for the actuator model and base motion, is proposed to get the required force information for control and design of ACM actuator. Second, a current shaping algorithm based on the ACM model is suggested in order to compensate for the performance degradation due to absence of feedback sensors without any side effects. Third, an engine vibration estimation algorithm, which uses such existing sensors as CAM and CAS, is extended to construct the gain map easily by applying an in-situ engine vibration estimation method using back EMF (electromotive force) of the actuator coil and engine-mounting system model. The prototype low-cost ACM construction is depicted in Fig. 2, which consists of three components: an ACM device, a current shaping controller and an engine vibration estimator. As a result, main difference between the low-cost ACM and full loaded ACM is absence of two feedback sensors, a displacement sensor for actuator control and a load cell for reference signal. To help understanding, cost comparison between the two is described in Table 1.

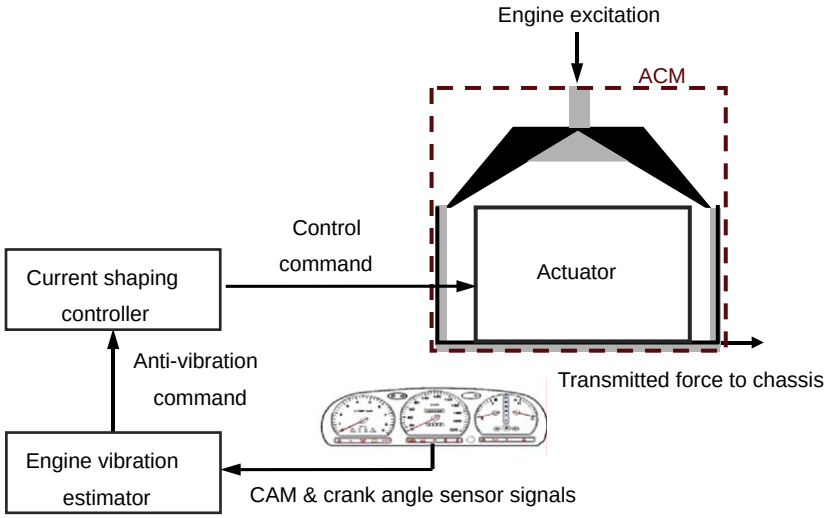

Fig. 2. Structure of the active control engine mount without feedback sensors.

Table 1
Cost comparison between the low-cost ACM and the full loaded ACM.

Components	Full loaded ACM ($)	Low-cost ACM ($)
Hydraulic mount	30	30
Current amplifier and micro-processor	100	100
Displacement sensor	2000	0
Load cell	100	0
Total	2230	130

3. Design and dynamic modeling of ACM

3.1. Design of ACM

Many researchers have considered the HEM as the basic structure for various types of active engine mount, mainly because of the inherent reliability in performance and the adaptability to new designs. As shown in Fig. 3, HEM has two force transfer paths: one through the main elastic rubber and another through the fluid in upper chamber. The elastic rubber exerts the force to the chassis, when it is vertically deformed by the engine, supporting the dynamic as well as static loads from the engine. Fluid in the chamber becomes functional when the pressure in the chamber is varied with the decoupler and the inertia track components. The inertia track supplies heavy damping force by resistance to the fluid motion. The decoupler provides amplitude dependent stiffness to compensate for the stiffness increase due to the upper chamber pressure.

The ACM, developed in the laboratory, employs the basic structure of the conventional HEM, of which upper chamber is connected to an actuator. The actuator, which essentially replaces the existing decoupler of the conventional passive HEM, actively controls the upper chamber pressure. By controlling the upper chamber pressure, the ACM can cancel the transmitted force from the engine to the chassis. The developed ACM is schematically depicted in Fig. 4.

3.2. Dynamic modeling of ACM

For effective design and control of an ACM system, an appropriate mathematical model is essential to describe both passive and active characteristics simultaneously. The passive characteristic means the dynamic behavior of ACM when the actuator is completely turned off. And the active characteristic describes the dynamic relationship between the actuator input and the vibration isolation of ACM.

The conventional HEM model, which has been proposed and optimized in the past by many researchers [26–33], was incorporated into the ACM model to describe the active as well as passive characteristics, accounting for dynamics of the active actuator. Lee and Lee [10] suggested a two-input single-output system as an ACM model, treating the engine vibration and the actuator runner displacement as the two independent inputs and the resulting transmitted force to the chassis as the output. The passive and active transfer functions, defined from the two-input single-output relationship, were extensively used for design and control of the ACM [10]. Sakamoto and Sakai [15] proposed a modified ACM model that reflects the actuator dynamics to explain the passive characteristics more precisely. They explained presence of the secondary mode

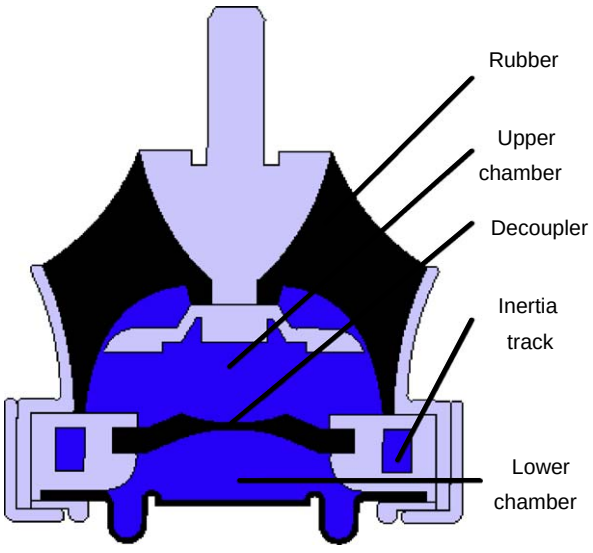

Fig. 3. Conventional hydraulic engine mount.

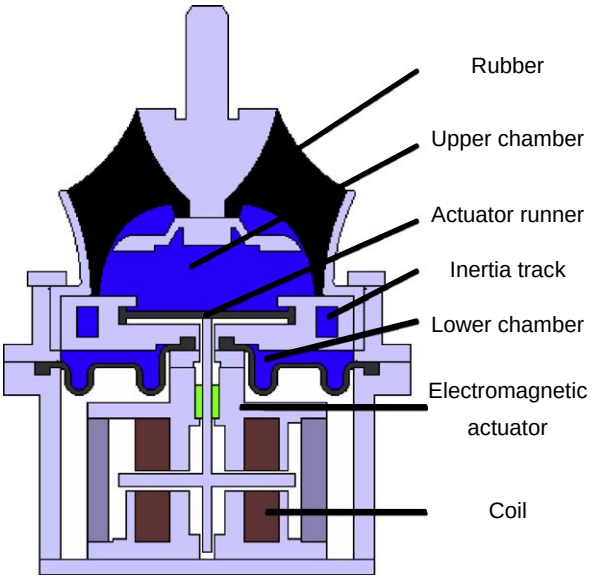

Fig. 4. The developed active control engine mount.

associated with the passive dynamic characteristics by including the actuator dynamics. However, inadequate modeling of the active control force led to the improper investigation of the active characteristics.

There are, at least, three critical problems with the previous ACM models. First, the actuator dynamics was not properly included in the ACM model, which could not properly explain the passive and active characteristics. Second, was made a simplistic, if not erroneous, assumption that the transmitted forces to the engine and the chassis are equal. It holds valid only if inertia effects in the ACM system are negligibly small, which plays an important role in ACM modeling. Finally, the dynamic characteristic of the actuator runner is better represented in terms of force rather than displacement.

In this paper, the concept of force transmissibility between the actuator control force and the transmitted force to engine or chassis is used to describe the active characteristics of ACM. In the previous works, the dynamic characteristics of ACM were derived from the model with its base, the chassis, fixed to the ground. This assumption means that the transmitted forces to the chassis and to engine are always identical to each other, regardless of the base vibration of the ACM. However, when mass elements are included in the ACM model, the dynamic stiffness and damping, and the active characteristics become quite different from those of the simplistic model.

A modified linear model, which accounts for the base motion and the actuator model, is shown in Fig. 5. The decoupler of conventional HEM is replaced by the runner of active actuator. Stiffness of active system accounts for the nonlinear stiffness of decoupler. The viscous damping coefficient of the decoupler is also replaced by damping coefficient of actuator. The active control force and relative reaction force are applied to the runner and the base of the ACM at each.

In Fig. 5, K_r and C_b represent the stiffness and volumetric compliance of rubber, respectively; A_c and A_t denote the cross-sectional areas of the actuator runner and the inertia track, respectively; A_e is the equivalent cross-sectional area of the upper fluid chamber. The fluid flow in the inertia track is modeled as the equivalent mass m_t and damping coefficient R_t, and the volumetric compliance of the lower chamber is designated as K_l. Because the fluid flows in the peripheral direction as complied with the track's geometry, the friction force against the fluid flow in the track is not directly transmitted to the chassis. Therefore, the inertia track is modeled such that it is connected to the absolute reference frame, not to the chassis. The active system is modeled as the runner mass m_c and damping coefficient R_c, and the stiffness of the actuator's mechanical spring is denoted by K_c. The active system is directly connected to the base of the ACM. From the model, the outputs, the force transmitted to the engine, $F_x(t)$, and the force transmitted to the chassis, $F_y(t)$, can be

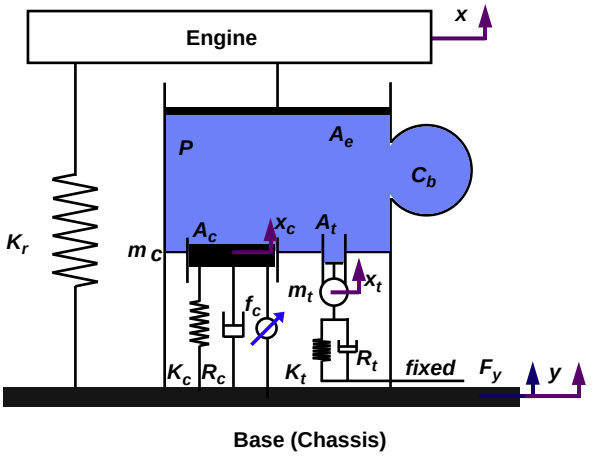

Fig. 5. New dynamic model for active control engine mount.

expressed as

$$F_x(t) = -K_r(x(t) - y(t)) + P(t)A_e \tag{1}$$

$$F_y(t) = K_r(x(t) - y(t)) - P(t)(A_e - A_c) + R_c(\dot{x}_c(t) - \dot{y}(t)) + K_c(x_c(s) - y(s)) - f_c(t) \tag{2}$$

The volumetric compliance element is deformed by the pressure in the upper chamber, i.e.

$$C_b = \frac{\Delta V_b}{P(t)} \tag{3}$$

The upper chamber pressure forces the fluid in the inertia track to flow and interacts with the active system, which can be written as

$$-A_t P(t) = m_t \ddot{x}_t(t) + R_t \dot{x}_t(t) + K_t x_t(t) \tag{4}$$

$$-A_c P(t) + f_c(t) = m_c \ddot{x}_c(t) + R_c(\dot{x}_c(t) - \dot{y}(t)) + K_c(x_c(t) - y(t)) \tag{5}$$

Using the fluid incompressibility assumption and the continuity equation, we have

$$A_e(x(t) - y(t)) + \Delta V_b = A_t x_t(t) + A_c(x_c(t) - y(t)) \tag{6}$$

From Eqs. (3)–(6), we can derive the upper chamber pressure as

$$\begin{aligned} P(s) = {} & \frac{-A_e(m_c s^2 + R_c s + K_c)(m_t s^2 + R_t s + K_t)}{A_c^2(m_t s^2 + R_t s + K_t) + A_t^2(m_c s^2 + R_c s + K_c) + C_b(m_t s^2 + R_t s + K_t)(m_c s^2 + R_c s + K_c)} X(s) \\ & + \frac{-(A_c m_c s^2 - A_e(m_c s^2 + R_c s + K_c))(m_t s^2 + R_t s + K_t)}{A_c^2(m_t s^2 + R_t s + K_t) + A_t^2(m_c s^2 + R_c s + K_c) + C_b(m_t s^2 + R_t s + K_t)(m_c s^2 + R_c s + K_c)} Y(s) \\ & + \frac{A_c(m_t s^2 + R_t s + K_t)}{A_c^2(m_t s^2 + R_t s + K_t) + A_t^2(m_c s^2 + R_c s + K_c) + C_b(m_t s^2 + R_t s + K_t)(m_c s^2 + R_c s + K_c)} f_c(s) \end{aligned} \tag{7}$$

From Eqs. (1)–(7), we can determine the transmitted forces to the engine, $F_x(t)$, and the base, $F_y(t)$, as

$$F_x(s) = -K_r(X(s) - Y(s)) + P(s)A_e = K_{xx}X(s) + K_{xy}Y(s) + T_{xc}f_c(s) \tag{8}$$

$$\begin{aligned} F_y(s) &= K_r X(s) - \left(K_r + \frac{m_c s^2(R_c s + K_c)}{m_c s^2 + R_c s + K_c}\right) Y(s) + \left(-A_e + \frac{A_c m_c s^2}{m_c s^2 + R_c s + K_c}\right) P(s) - \left(\frac{m_c s^2}{m_c s^2 + R_c s + K_c}\right) f_c(s) \\ &= K_{yx}X(s) + K_{yy}Y(s) + T_{yc}f_c(s) \end{aligned} \tag{9}$$

Finally, the dynamics characteristics of ACM can be re-expressed in the matrix form as

$$\begin{bmatrix} F_x(s) \\ F_y(s) \end{bmatrix} = \begin{bmatrix} -K_{xx}(s) & K_{xy}(s) & T_{xc}(s) \\ K_{yx}(s) & -K_{yy}(s) & T_{yc}(s) \end{bmatrix} \begin{bmatrix} X(s) \\ Y(s) \\ f_c(s) \end{bmatrix} \tag{10}$$

where

$$K_{xx}(s) = -K_r - \frac{A_e^2(m_c s^2 + R_c s + K_c)(m_t s^2 + R_t s + K_t)}{A_c^2(m_t s^2 + R_t s + K_t) + A_t^2(m_c s^2 + R_c s + K_c) + C_b(m_t s^2 + R_t s + K_t)(m_c s^2 + R_c s + K_c)}$$

$$K_{xy}(s) = K_r - \frac{(A_e A_c m_c s^2 - A_e^2(m_c s^2 + R_c s + K_c))(m_t s^2 + R_t s + K_t)}{A_c^2(m_t s^2 + R_t s + K_t) + A_t^2(m_c s^2 + R_c s + K_c) + C_b(m_t s^2 + R_t s + K_t)(m_c s^2 + R_c s + K_c)}$$

$$K_{yx}(s) = K_r - \frac{(A_e A_c m_c s^2 - A_e^2(m_c s^2 + R_c s + K_c))(m_t s^2 + R_t s + K_t)}{A_c^2(m_t s^2 + R_t s + K_t) + A_t^2(m_c s^2 + R_c s + K_c) + C_b(m_t s^2 + R_t s + K_t)(m_c s^2 + R_c s + K_c)}$$

$$K_{yy}(s) = -\left(K_r + \frac{m_c s^2(R_c s + K_c)}{m_c s^2 + R_c s + K_c}\right) + \frac{(A_e(m_c s^2 + R_c s + K_c) - A_c m_c s^2)(A_c m_c s^2 - A_e(m_c s^2 + R_c s + K_c))(m_t s^2 + R_t s + K_t)}{(m_c s^2 + R_c s + K_c)(A_c^2(m_t s^2 + R_t s + K_t) + A_t^2(m_c s^2 + R_c s + K_c) + C_b(m_t s^2 + R_t s + K_t)(m_c s^2 + R_c s + K_c))}$$

$$T_{xc}(s) = \frac{A_e A_c(m_t s^2 + R_t s + K_t)}{A_c^2(m_t s^2 + R_t s + K_t) + A_t^2(m_c s^2 + R_c s + K_c) + C_b(m_t s^2 + R_t s + K_t)(m_c s^2 + R_c s + K_c)}$$

$$T_{yc}(s) = -\frac{m_c s^2}{m_c s^2 + R_c s + K_c} - \frac{(m_t s^2 + R_t s + K_t)(A_e A_c(m_c s^2 + R_c s + K_c) - A_c^2 m_c s^2)}{(m_c s^2 + R_c s + K_c)(A_c^2(m_t s^2 + R_t s + K_t) + A_t^2(m_c s^2 + R_c s + K_c) + C_b(m_t s^2 + R_t s + K_t)(m_c s^2 + R_c s + K_c))} \tag{11}$$

Here, $K_{xx}(s)$, $K_{xy}(s)$, $K_{yx}(s)$ and $K_{yy}(s)$ are the passive dynamic characteristics, and, $T_{xc}(s)$ and $T_{yc}(s)$ describe the active dynamic characteristics of ACM. The spring constant, K_r, appearing in the passive dynamic characteristics, $K_{xx}(s)$, $K_{xy}(s)$, $K_{yx}(s)$ and $K_{yy}(s)$, implies that the ACM can support the static load from the engine. In contrast to the passive characteristics, the active characteristics, $T_{xc}(s)$ and $T_{yc}(s)$, have the complex conjugate zeros near the origin of the s-plain due to the small bulge stiffness of the lower chamber K_t. It implies that the actuator does not bear the static force from the engine. The zeros of the six transfer functions are determined by the inertia track and actuator components, while the poles are determined by the inertia track and actuator components, and, the volumetric compliance of rubber.

On the other hand, the transmitted force to the chassis is also derived from the conventional model in Fig. 6 as [10,15]. Note that the assumption of $T_{yc}(s) = Y(s) = 0$ in Eq. (10) reduces to Eq. (12):

$$F_y(s) = F_x(s) = K_{xx}(s)X(s) + T_{xc}(s)f_c(s) \tag{12}$$

An experimental apparatus for measurement of dynamic characteristic of ACM is shown in Fig. 7, where the test ACM is installed on a computer controlled servo-hydraulic actuation system (INSTRON dynamic material testing system, model 8502). The excitation displacement, which simulates the engine and chassis vibrations, is measured by an LVDT. The two load cells that are installed at the top and bottom sides of the test ACM measure the transmitted forces to the engine and chassis. The measured displacement and force signals are fed to signal conditioners and post-processed to compute the passive transfer functions such as $K_{xx}(s)$, $K_{xy}(s)$, $K_{yx}(s)$ and $K_{yy}(s)$ in Eq. (10). The current to the coil of the electromagnetic actuator is also measured to calculate the actuator control force. Then, the control force and the transmitted forces are processed to find out the active transfer functions, $T_{xc}(s)$ and $T_{yc}(s)$. Tables 2 and 3 show the properties of the

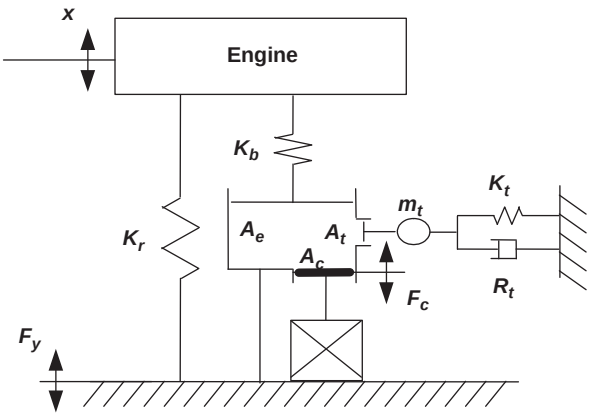

Fig. 6. Conventional dynamic model for active control engine mount [10,15].

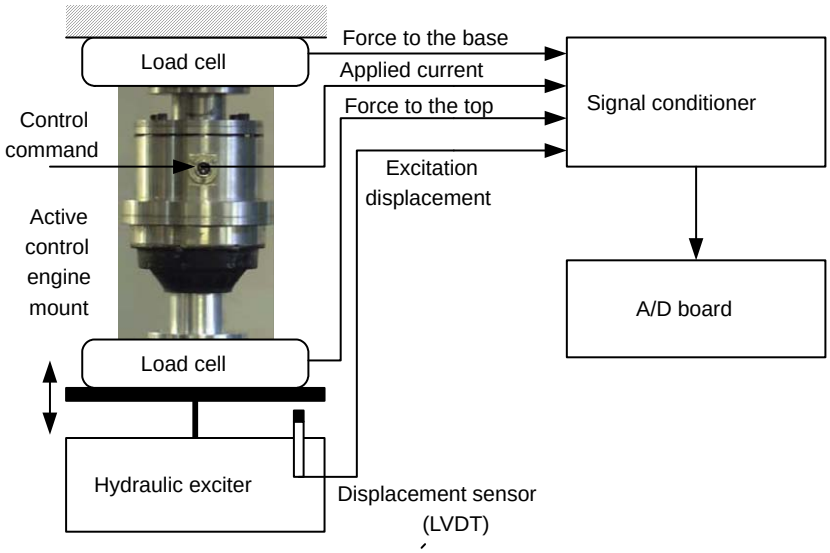

Fig. 7. Experimental setup for model identification.

Table 2
Parameters of the prototype ACM.

Symbol	Name	Value
K_r	Main stiffness	1.6×10^5 N/m
C_b	Volumetric compliance	5.0×10^{-11} m^3/N
K_c	Stiffness of actuator	1.14×10^5 N/m
K_t	Bulge stiffness of diaphragm	1 N/m
A_e	Equivalent piston area of rubber	3337 mm^2
A_c	Decoupler area	1256 mm^2
A_t	Cross-sectional area of inertia track	20 mm^2
m_t	Fluid mass of inertia track	5.1 g
m_c	Mass of actuator runner	78.5 g
R_t	Damping coefficient in the inertia track	0.18 N s/m
R_c	Damping coefficient of actuator	100 N s/m
ρ	Fluid density	1050 kg/m^3
–	Height of ACM	135 mm
–	Diameter of ACM	100 mm

Table 3
Parameters of the electromagnetic actuator.

Symbol	Name	Value
μ_0	Absolute permeability	$4\pi \times 10^{-7}$ Wb/A m
N	Number of coil turns	400 turns
I_{max}	Maximum current	4 A
A_p	Pole face area	268 mm^2
g_0	Nominal air gap	1.5 mm
L	Coil inductance	10 mH
R	Coil resistance	4 Ω

prototype ACM and the electromagnetic actuator, respectively. For experimental estimation of the active and passive transfer functions of the prototype ACM, a series of harmonic tests were performed. During the harmonic tests, the frequency was varied from 1 to 100 Hz and the dynamic amplitudes of the harmonic displacement excitations and currents were kept to be 0.1 mm and 2 A, respectively.

Fig. 8 compares the experiment and simulation results for the passive and active dynamic transfer functions. Note that the new simulation results, based on the newly proposed ACM model and, the experimental ones are in agreement with fair accuracy. The control target of ACM is to reduce the transmitted force to the chassis, then transmissibility between the actuator force and transmitted force to the base, T_{yc}, should be mainly described by a model. However the old model, proposed by Lee [10], calculates transmissibility of ACM with several assumptions: (1) fluid in the chamber is incompressible, (2) transmitted force to the upper side (F_x, engine side) equals to the transmitted force to the lower side (F_y, chassis side). With these assumptions, transmissibility of the model-old describes only the T_{xc} as described in Fig. 8(c). In the enhanced model proposed in this paper, The assumption (2) is no longer valid for the actuator model is included in the ACM model. By this modification of ACM model, the model-new can describe the T_{yc} directly as shown in Fig. 8(c). Comparing the old and new models, four dynamic stiffnesses of the ACM, described in Figs. 8(a) and (b), are not much different from each other, but the active transfer functions in Fig. 8(c) show significant difference, which results essentially from the inertia effect of actuator runner. It implies that the actuator runner inertia becomes important in design and control of actuator, particularly in calculation of the required actuator control force. Note that the new model is adequate to predict both the passive and active characteristics of the ACM in the design and control stage.

4. Current shaping control

The electromagnetic force generated by a Maxwell force type actuator, shown in Fig. 9, becomes

$$f_c = \frac{\mu_0 N^2 I_1^2 A_p}{4(g_0 - x_r)^2} - \frac{\mu_0 N^2 I_2^2 A_p}{4(g_0 + x_r)^2} \tag{13}$$

where μ_0 is the absolute permeability, N is the number of coil turns, I_1 and I_2 are the applied currents to a pair of facing coils, A_p is the pole face area, g_0 is the nominal air gap and x_r represents the relative runner displacement to the base. The Maxwell type electromagnetic force has two inherent control problems, the nonlinearity with respect to the input currents and the harmonic distortion by runner movements, which cannot be readily resolved without feedback control [16–21]. Fig. 10 shows the typical measured control force of ACM for the sinusoidal input currents. To isolate the primary engine harmonic vibration, which is induced by the transmitted force related to an engine speed, actuator has to generate the desired harmonic force of the corresponding frequency. As shown in Fig. 10, the actuator force due to the harmonic current input is not of a

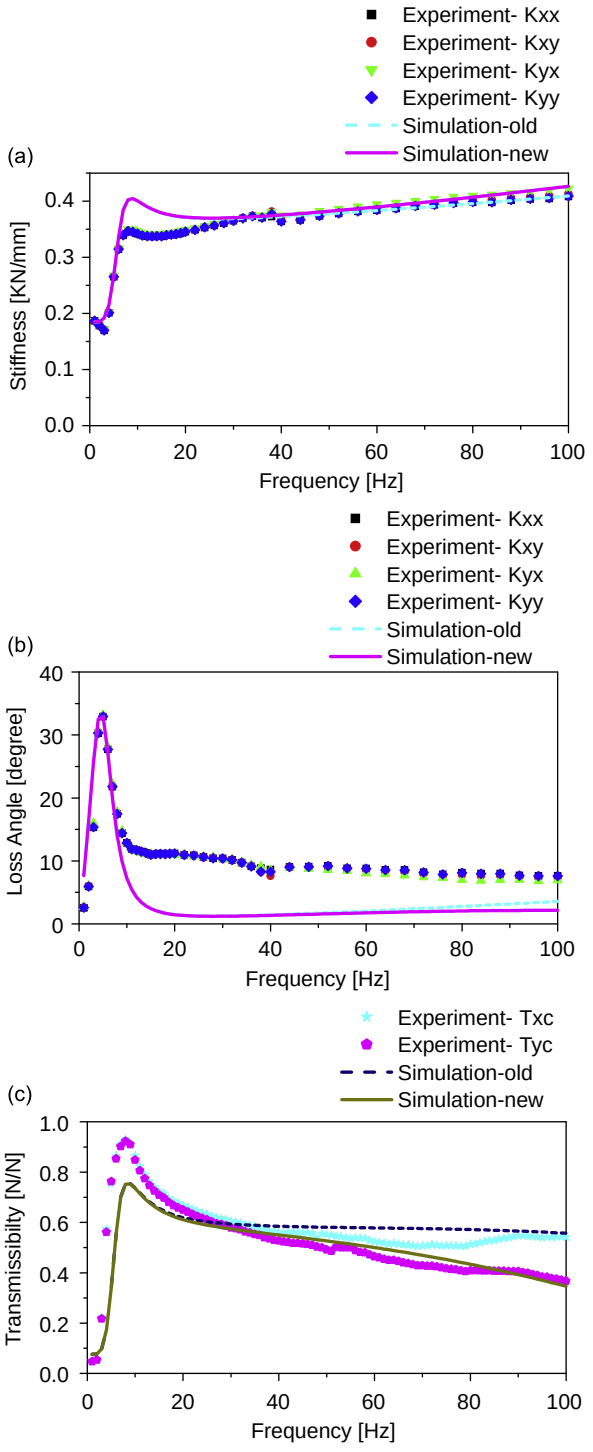

Fig. 8. Transfer functions of ACM: (a) dynamic stiffness, (b) loss angle and (c) force transmissibility.

pure harmonic type, but its waveform is distorted, resulting in undesired vibrations of higher harmonics transmitted to the chassis.

Input shaping is a well-known technique in vibration control of structures and robots, which effectively suppresses the motion-induced vibration of structure, especially the residual vibrations of structures and

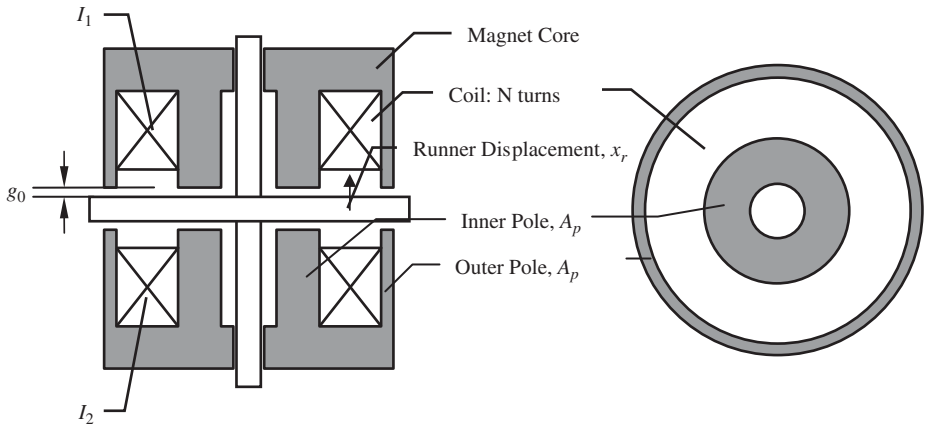

Fig. 9. Structure of electromagnetic actuator [10].

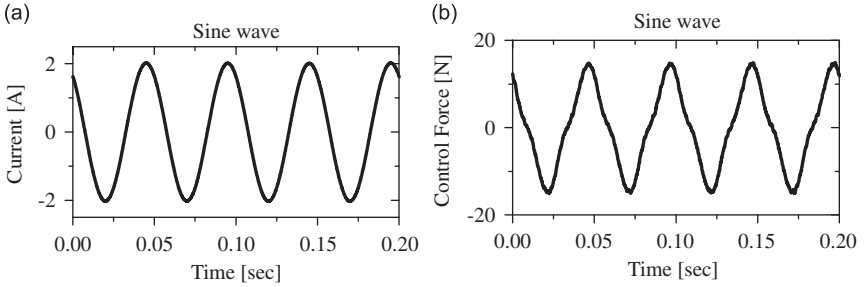

Fig. 10. (a) Harmonic current input and (b) the resulting distorted control force.

manipulators [22–25]. The technique can also be used for the harmonic force generation of actuator by properly shaping the input command signal using the known actuator model.

For the harmonic force, $f_c(t) = F^* \sin(\Omega t + \phi)$, applied to the actuator runner, the equation of actuator runner motion is given by

$$f_c(t) = F^* \sin(\Omega t + \phi) = m_c \ddot{x}_c + \left(K_c + \frac{A_c^2}{C_b}\right) x_c \tag{14}$$

where F, Ω and ϕ are the magnitude, frequency and phase, respectively, of the desired harmonic control force. Eq. (14) yields

$$x_c(t) = \frac{F}{\left\{\left(K_c + \frac{A_c^2}{C_b}\right) - \Omega^2 m_c\right\}} \sin(\Omega t + \phi) \tag{15}$$

The electromagnetic force is derived from Eq. (13) as

$$f_c = F^* \sin(\Omega t + \phi) = \frac{\mu_0 N^2 I_1^2 A_p}{4(g_0 - x_c)^2} - \frac{\mu_0 N^2 I_2^2 A_p}{4(g_0 + x_c)^2} \tag{16}$$

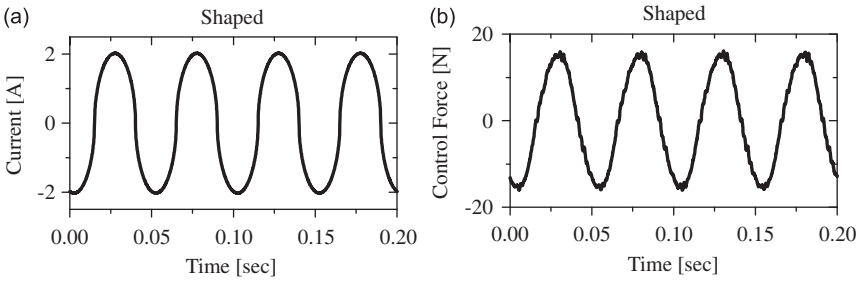

Fig. 11. (a) Shaped current input and (b) the resulting almost harmonic control force.

Using Eqs. (14)–(16), the shaped input command required to compensate for harmonic distortion due the nonlinearity and runner movement can be derived as

$$I_1(t)=\begin{cases}\sqrt{\dfrac{4F\left|\sin(\Omega t+\phi)\right|}{\mu_0 N^2 A_p}}\left\{g_0-\dfrac{F}{\left\{\left(K_c+\dfrac{A_c^2}{C_b}\right)-\Omega^2 m_c\right\}}\sin(\Omega t+\phi)\right\} & (0\leqslant t+2n\pi\leqslant\pi)\\ 0 & (\pi\leqslant t+2n\pi\leqslant 2\pi)\end{cases} \tag{17}$$

$$I_2(t)=\begin{cases}0 & (0\leqslant t+2n\pi\leqslant\pi)\\ \sqrt{\dfrac{4F\left|\sin(\Omega t+\phi)\right|}{\mu_0 N^2 A_p}}\left\{g_0+\dfrac{F}{\left\{\left(K_c+\dfrac{A_c^2}{C_b}\right)-\Omega^2 m_c\right\}}\sin(\Omega t+\phi)\right\} & (\pi\leqslant t+2n\pi\leqslant 2\pi)\end{cases} \tag{18}$$

Fig. 11 shows the measured control force for the applied current of ACM when the current input command is shaped according to Eqs. (17) and (18). Comparison of Figs. 10 and 11 confirms that the current shaping control significantly improves the harmonic distortion of the control force.

5. Engine vibration estimation

To generate the control force by the actuator counter-acting to the engine-induced force, the reference signal, the so-called anti-vibration signal, associated with the engine vibration is essential for the ACM system. In the recent decade, the estimation techniques of engine torque using measurement of crankshaft speed variation were introduced for improved engine diagnostics and control [12–14]. The proposed ACM without feedback sensors is only capable of isolating the main harmonic component of the engine-induced vibration that corresponds to the cylinder firing frequency. The actuator of the proposed ACM requires the information of frequency (Ω), phase (Φ) and amplitude (F) of the main harmonic vibration of engine only, in order to generate the counteracting vibration as expressed in Eq. (16).

Fig. 12 describes the estimation scheme of the main harmonic engine vibration. The engine torque generated by ignition drives the crankshaft, whose rotation is measured by CAS at the flywheel location. The dynamic combustion torque also forces the engine-mounting system to vibrate and transmit force to the chassis. Using the force transmissibility of ACM, the transmitted force to the chassis and thus the anti-vibration command are determined. The engine motion due to the combustion torque can be expressed as

$$T_e(s)=\{[M]s^2+[C]s+[K]\}q(s) \tag{19}$$

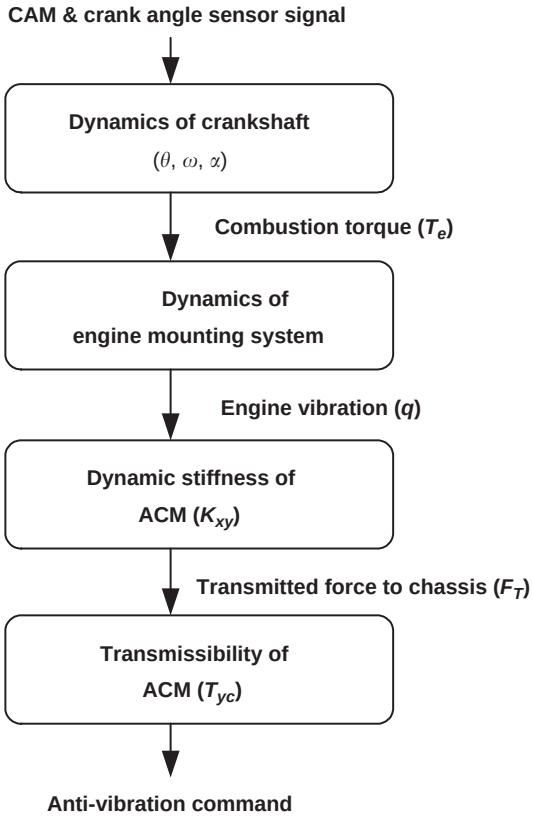

Fig. 12. Engine vibration estimation using CAM and CAS signal.

where $q(s)$ is the displacement vector of the mass center of engine given as

$$q(s) = [x(s)\ \ y(s)\ \ z(s)\ \ \theta_x(s)\ \ \theta_y(s)\ \ \theta_z(s)]^T \tag{20}$$

Here, $[M]$, $[C]$ and $[K]$ are the mass, damping and stiffness matrices of the engine-mounting system, respectively.

When the engine idles or drives, the main harmonic frequency of the engine-induced vibration becomes much higher than the natural frequencies of the engine-mounting system. Thus, Eq. (19) reduces to

$$T_e(s) \cong [M]s^2 q(s) \tag{21}$$

The transmitted force through engine mounts, F_T, becomes

$$F_T(s) = \{[C]s + [K]\}q(s) \tag{22}$$

From Eqs. (21) and (22), we can derive

$$F_T(s) \cong \frac{\{[C]s + [K]\}}{[M]s^2} T_e(s) \tag{23}$$

implying that the transmitted force from engine to chassis is directly related to the engine combustion torque. By the force transmissibility of the ACM system, the anti-vibration command signal to cancel out the transmitted force through ACM can be calculated from

$$f_c(s) = -T_{yc}(s)F_T(s) \cong -T_{yc}(s)\frac{\{[C]s + [K]\}}{[M]s^2} T_e(s) \tag{24}$$

Giorgio [13] suggested that the rotating motion of crankshaft can be modeled as an equivalent circuit given as [13]

$$T_e(s) = \left[L_e + \frac{1}{Cs^2} + \frac{R_e + R_c}{s}\right]\alpha(s) \cong L_e\alpha(s) \tag{25}$$

where L_e means the equivalent inertia of the crankshaft, flywheel, clutch and valve train, and, C, R_e and R_c represent the stiffness, crankshaft journal bearing damping and clutch damping, respectively [13]. The simple approximate relation in Eq. (25) is valid since the stiffness and damping effects are far smaller than the inertia effect over the frequency range of interest [13,14]. The approximate relations given in Eqs. (23) and (25)

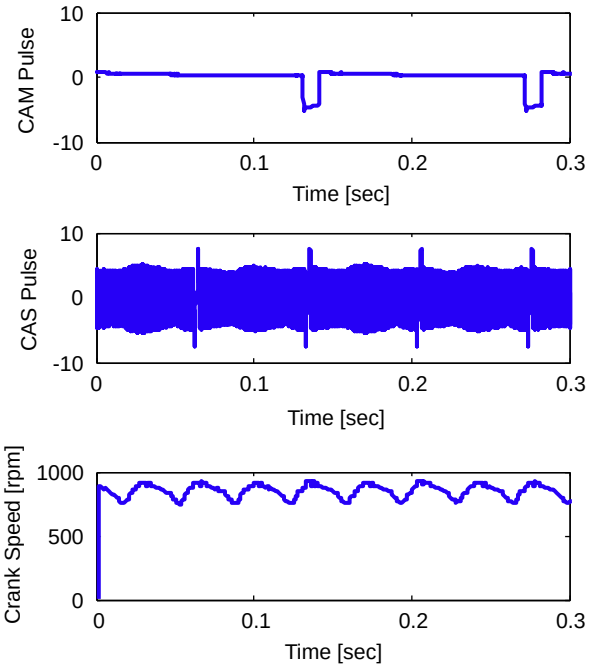

Fig. 13. Typical signals: (a) CAM pulse, (b) crank pulse and (c) angular speed of crankshaft.

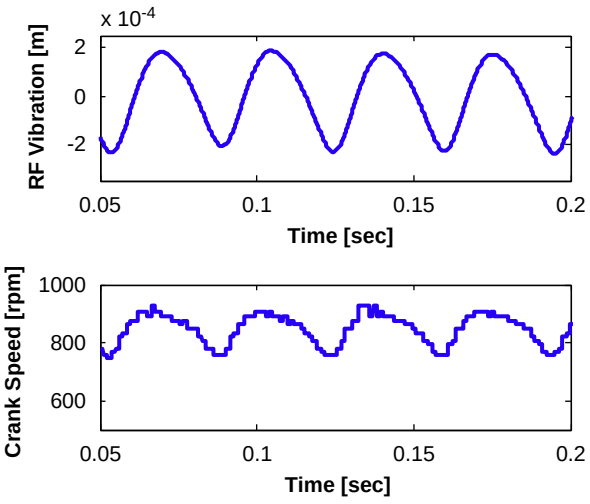

Fig. 14. (a) Roll front vibration and (b) angular velocity of crankshaft.

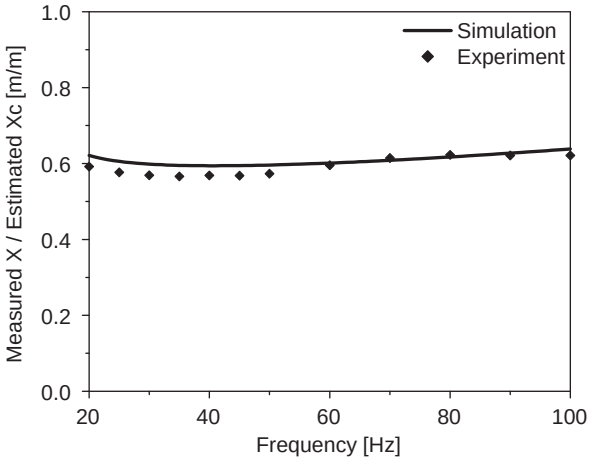

Fig. 15. Transfer function between measured engine vibration and estimated runner vibration.

suggest that the engine combustion torque, $T_e(s)$, can be well estimated from measurement of the crankshaft angular acceleration by CAS, and the transmitted force though engine mounts, F_T, can be also approximately estimated from the CAS signal.

Figs. 13(a) and (b) show the typical crank angle and CAM signals, respectively, when the engine idles with gear drive at '*D*'. The angular speed of crankshaft can be easily derived from the CAS signal, as illustrated in Fig. 13(c). Fig. 14 confirms the fact that the engine vibration measured at the roll mount position resembles the derived angular speed variation. Therefore, by detecting the fluctuations in crankshaft speed, we can estimate the magnitude and phase of engine vibration in reference to the timing of CAM pulse. From Fig. 12, it can be concluded that the gain between the engine vibration and anti-vibration command is obtained from the proposed ACM model. But, here still remains a problem that we should find the gain between the engine vibration and angular speed.

In an electromagnetic system, it is well known that the inductance of electromagnet is inversely proportional to the air gap, which varies with the runner displacement [34–37], and its relationship is given as [34]

$$x_c = g_0 \pm \frac{1}{2}\mu_0 N^2 A_p \omega_c \left|\frac{I_c}{V_c}\right| \tag{26}$$

where x_c is the actuator runner displacement, ω_c, I_c, V_c are the frequency, applied current and back emf voltage, respectively, of the carrier wave introduced to estimate the runner displacement. From Eq. (26), the actuator runner movement can be estimated from the back emf voltage measurement. Fig. 15 shows the relationship between the engine vibration, x, and runner displacement, x_c, which can be derived from the ACM model as

$$\frac{X_c}{X}(s) = \frac{A_e A_c (m_t s^2 + R_t s + K_t)}{[A_c^2(m_t s^2 + R_t s + K_t) + A_t^2(m_c s^2 + R_c s + K_c) + C_b(m_t s^2 + R_t s + K_t)(m_c s^2 + R_c s + K_c)]} \tag{27}$$

From this observation, by estimating the engine vibration, the gain between the angular speed and engine vibration can be well estimated by in-situ experiments without any additional sensors.

6. Vibration isolation performance of ACM system

To evaluate the vibration isolation performance of the proposed ACM system, uni-directional vibration isolation tests were carried out, using the experimental setup shown in Fig. 16. The test ACM was excited by a hydraulic material testing machine that simulates the actual engine vibration, while the transmitted force and excitation displacement were measured by a force transducer and an LVDT sensor, respectively. To control the ACM system, a commercial real time controller (dSPACE) was used, while the ACM controller provided

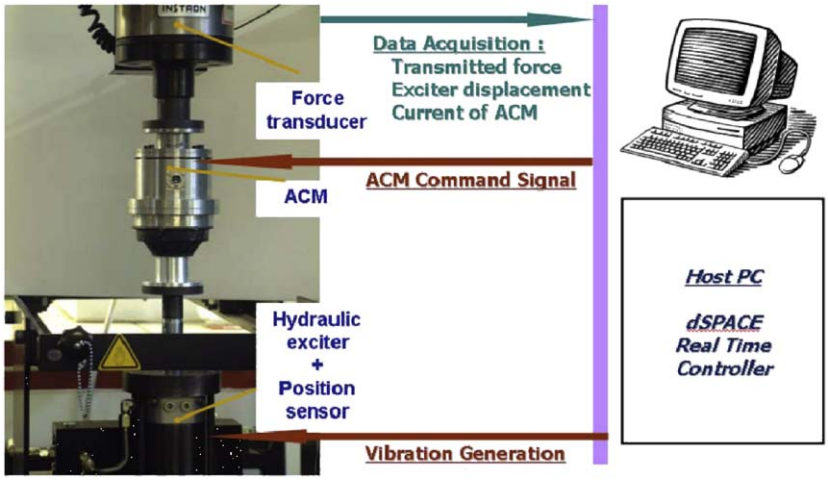

Fig. 16. Experimental setup for vibration isolation tests.

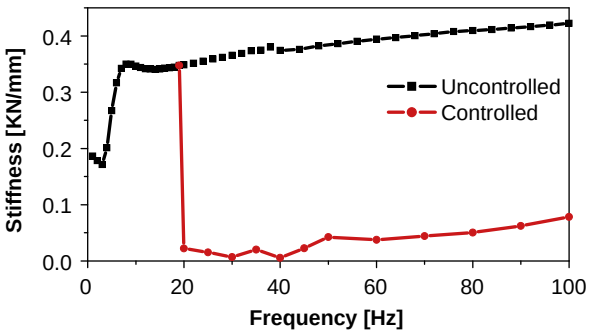

Fig. 17. Equivalent dynamic stiffness of ACM.

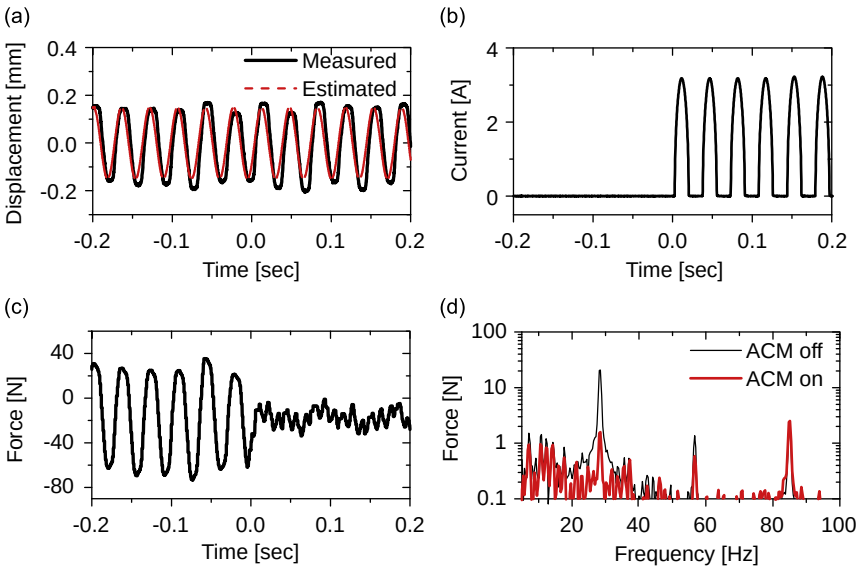

Fig. 18. Experimental results: (a) vibration displacement of ACM (solid: engine vibration, dot: estimated vibration), (b) applied current to coil, (c) transmitted forces (time domain) and (d) transmitted forces (frequency domain).

model based control commands from the estimated engine vibration signals to attenuate the transmitted forces via ACM.

As a measure for vibration isolation performance of the ACM, dynamic stiffness was measured, when the ACM was excited by a series of harmonic base displacement of frequency ranging from 1 to 100 Hz with 0.1 mm in amplitude, as the activation of the ACM actuator was limited in frequency between 20 and 100 Hz. Fig. 17 shows that the dynamic stiffness of the ACM with its control on is reduced to, at least, $\frac{1}{4}$ of its passive stiffness over the frequency ranges of control.

To simulate the vehicle test of the prototype ACM, the engine vibration at the roll front position was exerted to the ACM by the hydraulic exciter in Fig. 16. To provide the engine-simulated vibration, the vibration displacement of engine at each mounts, CAM pulse and CAS pulse were measured simultaneously from a test vehicle which had a 2.0 l 4-cylinder 4-cycle in-line engine combined with an automatic transmission, which is transversely mounted at four mounting positions. The ACM controller generated the control commands from the CAM and CAS signals, while the hydraulic exciter simulated the engine vibration displacement.

The vibration isolation performance tests were carried out by simulating the engine idle shake. Fig. 18(a) describes the vibration displacements of the ACM, which simulates the engine-mount vibration, and the estimated engine vibration from the CAS and CAM signals. Figs. 18(b) show the applied current signal that is shaped by current control. Figs. 18(c) and (d) illustrate the transmitted force through the ACM and its FFT results, when the ACM was initially off and turned on at $t = 0$ s. At the firing frequency, the transmitted main harmonic force was reduced by 20 dB, which is considered to be a significant improvement in reducing vibration in automobiles. But, the force of higher harmonics was even a little increased or passed without change because the ACM is capable of only the main harmonic component. It leads to reduction of the RMS (root mean square) value of the transmitted force by 13 dB, referring to Fig. 18. Note that the proposed ACM, using the current shaper and vibration estimator, isolates the transmitted force to the chassis by more than 13 dB.

Target frequency range of ACM is decided 20–100 Hz to control the main harmonic vibration of engine between idle and 3000 rev/min. At the low frequency, the ACM can isolate the vibrations over than 20 dB, but in high frequency range, the vibration isolation performance is limited by the sampling frequency of the controller. In the vibration isolation test, we use the controller having the 5 kHz, and this means that the controller has at least 7.2° phase errors. By the phase estimation errors of vibration estimation algorithm due to sampling frequency, vibration isolation performance of ACM is limited about 13 dB over the frequency range of 20–100 Hz.

7. Conclusions

A prototype low-cost ACM is developed without feedback sensors, and its improved model and model based feed forward algorithm were proposed. To construct a low-cost ACM system, all feedback sensors normally required for full ACM systems were replaced by the model based feed forward algorithm, consisting of improved ACM model, current shaping controller and the vibration estimation algorithm.

To investigate the dynamic characteristics of the ACM and offer the useful information for the ACM design and model based feed forward control such as the force transmissibility, an improved ACM model, which includes the passive and active dynamic characteristics of the ACM, was proposed and mathematically analyzed. To solve the inherent instability problem and force control problems, a pair of mechanical springs was used to stabilize the Maxwell force type actuator without feedback sensor, and the current shaping technique was used for the harmonic force generation of actuator by properly shaping the input command signal using the known actuator model. To get the anti-vibration signal, which was essential for counter-acting control force generation, an engine vibration estimator using measurement of crankshaft speed variation was developed. The engine vibration estimator provided the information of frequency (Ω), phase (Φ) and amplitude (F) of the main harmonic vibration of engine, in order to isolate main harmonic component of the engine-induced vibration that corresponded to the cylinder firing frequency.

Uni-directional vibration isolation tests were carried out to evaluate the vibration isolation performance of the proposed ACM system. The experimental results proved that the cost-effective ACM without feedback sensors was able to reduce the transmitted force to the chassis less than $\frac{1}{5}$ of passive state.

Acknowledgment

The authors gratefully acknowledge the Next Generation Vehicle Technology Co., South Korea, for supporting this research.

References

[1] D.M. Ford, An analysis and application of a decoupled engine mount system for idle isolation, *SAE Transactions* 850976 (1985).
[2] H. Hata, H. Tanaka, Experimental method to derive optimum engine mount system for idle shake, *SAE Transactions* 870961 (1987).
[3] Y.T. Choi, S.B. Choi, C.C. Cheong, Performance analysis of an engine mount featuring ER fluid and piezo-actuators, *International Journal of Modern Physics B* 10 (23) (1996) 3143–3159.
[4] J. Nakhaie, G. Farid, Engine mounts for automotive applications: a survey, the shock and vibration digest, September, 2002, pp. 363–379.
[5] H. Ozaki, T. Tsukamoto, A. Ichikawa, H. Yamazoe, A. Shibata, T. Maeno, H. Tajima, Development of active engine mount, *JSAE Annual Congress*, 1999, pp. 141–144.
[6] H. Haldenwanger, P. Klose, Isolation and compensation of vibration by means of active piezo-ceramic mounts, *Proceedings of Advanced Vehicle Control*, 1992, pp. 23–27.
[7] S. Ushijima, S. Jumakawa, Active engine mount with piezo-actuator for vibration control, *SAE Transaction* 930201 (1993).
[8] A. Gennesseaux, Research for new vibration techniques: from hydro-mount to active mounts, *SAE Proceedings of Noise and Vibration Conference*, 1993, pp. 491–499.
[9] Y. Nakaji, S. Satoh, T. Kimura, T. Hamabe, Y. Akatsu, H. Kawazoe, Development of an active control engine mount system, *Vehicle System Dynamics* 32 (1999) 185–193.
[10] Y.W. Lee, C.W. Lee, Dynamic analysis and control of active engine mount system, *Journal of Automobile Engineering* 216 (11) (2002) 921–931.
[11] K. Aoki, T. Shikata, T. Hyoudou, T. Hirade, T. Aihara, Application of an active control mount (ACM) for improved diesel engine vehicle quietness, *SAE Transactions* 1999-01-0832 (1999).
[12] M. Hideki, T. Mikasa, H. Nemoto, NV Countermeasure technology for a cylinder-on-demand engine—development of active control engine mount, *SAE Transactions* 2004-01-0413 (2004).
[13] R. Giorgio, Estimate of indicated torque from crankshaft speed fluctuations: a model for the dynamics of the IC engine, *IEEE Transactions on Vehicular Technology* 38 (3) (1989) 168–179.
[14] B.H. Lee, R. Giorgio, Y. Guezennec, A. Soliman, M. Cavalletti, W. James, Engine control using torque estimation, *SAE Transactions* 2001-01-0995 (2001).
[15] K. Sakamoto, T. Sakai, Development of simulation model for active control engine mount, *JSAE Review of Automotive Engineering* 27 (2006) 155–157.
[16] H.Y. Kim, C.W. Lee, Design and control of active magnetic bearing system with Lorentz force-type axial actuator, *Mechatronics* 16 (1) (2005) 13–20.
[17] H.Y. Kim, C.W. Lee, Analysis of eddy-current loss for design of small active magnetic bearings with solid core and rotor, *IEEE Transactions on Magnetics* 40 (5) (2004) 3293–3301.
[18] W.S. Han, C.W. Lee, Y. Okada, Design and control of a disk type integrated motor-bearing system, *IEEE/ASME Transactions on Mechatronics* 7 (1) (2002) 15–22.
[19] S.J. Kim, C.W. Lee, On-line identification of current and position stiffnesses based on LMS algorithm for active magnetic bearing system equipped with force transducers, *Mechanical Systems and Signal Processing* 13 (5) (1999) 681–690.
[20] S.J. Kim, C.W. Lee, Diagnosis of sensor faults in active magnetic bearing system equipped with built-in force transducers, *IEEE/ASME Transactions on Mechatronics* 4 (2) (1999) 180–186.
[21] B.H. Lee, M.B. Park, Y.W. Lee, C.W. Lee, Design of the current feedback electromagnetic actuator for engine vibration control, *The 32nd International Congress and Exposition on Noise Control Engineering* (*Inter-Noise*), Jeju, Korea, 2003, pp. 355–359.
[22] J.Y. Park, P.H. Chang, Vibration control of a telescopic handler using time delay control and commandless input shaping technique, *Control Engineering Practice* 12 (2004) 769–780.
[23] W. Singhose, L. Porter, M. Kenison, E. Kriikku, Effects of hoisting on the input shaping control of gantry cranes, *Control Engineering Practice* 8 (2000) 1159–1165.
[24] T.S. Yang, K.S. Chen, C.C. Lee, J.F. Yin, Suppression of motion-induced residual vibration of a cantilever beam by input shaping, *Journal of Engineering Mathematics* 54 (2006) 1–15.
[25] J.J. Shan, H.T. Liu, D. Sun, Modified input shaping for a rotating single-link flexible manipulator, *Journal of Sound and Vibration* 285 (2005) 187–207.

[26] J.E. Colgate, C.T. Chang, Y.C. Chiou, W.K. Liu, L.M. Keer, Modeling of a hydraulic engine mount focusing on response to sinusoidal and composite excitations, *Journal of Sound and Vibration* 184 (1995) 503–528.
[27] A.A. Geisberger, A. Khajepour, M.F. Golnaraghi, Nonlinear modeling of hydraulic mounts theory and experiment, *Journal of Sound and Vibration* 249 (2) (2002) 371–397.
[28] G. Kim, R. Singh, A study of passive and adaptive hydraulic engine mount systems with emphasis on non-linear characteristics, *Journal of Sound and Vibration* 179 (1995) 427–453.
[29] R. Singh, G. Kim, P. Ravindra, Linear analysis of automotive hydro-mechanical mount with emphasis on decoupler characteristics, *Journal of Sound and Vibration* 158 (2) (1992) 219–243.
[30] M.S. Foumani, A. Khajepour, M. Durali, Application of sensitivity analysis to the development of high performance adaptive hydraulic engine mounts, *Vehicle System Dynamics* 39 (4) (2003) 257–278.
[31] J. Christopherson, J. Nakhaie, Optimization of classical hydraulic engine mounts based on RMS method, *Shock and Vibration* 12 (2005) 119–149.
[32] Y.K. Ahn, J.D. Song, B.S. Yang, K.K. Ahn, S. Morishita, Optimal design of nonlinear hydraulic engine mount, *Journal of Mechanical Science and Technology* 19 (3) (2005) 768–777 (formerly KSME International Journal).
[33] J. Christopherson, J. Nakhaie, Dynamic behavior comparison of passive hydraulic engine mounts. Part 1: mathematical analysis, *Journal of Sound and Vibration* 290 (2006) 1040–1070.
[34] K.S. Kwon, H.S. Jeong, C.W. Lee, Displacement sensorless magnetic bearing control by current measurement, *Proceedings of KSME Spring Conference*, 1994, pp. 655–658.
[35] C.H. Choi, K.H. Park, Self-sensing magnetic levitation using a LC resonant circuit, *Sensors and Actuators—Physical* 72 (1999) 169–177.
[36] K. Matsuda, Y. Okada, Self-sensing magnetic bearing using the principle of differential transformer, *Proceedings of the Fifth International Symposium on Magnetic Bearings*, 1996, pp. 109–112.
[37] M.D. Noh, M.K. Jeong, Development of a low cost inductive sensor using switching noise demodulation, *The Eighth International Symposium on Magnetic Bearing*, 2002, pp. 311–314.